Asian Journal of Chemistry; Vol. 38, No. 11 (2026), 3097-3106
ASIAN JOURNAL OF CHEMISTRY
https://doi.org/10.14233/ajchem.2026.36990

Efficient and Reusable Polymer Supported Copper(II) and Vanadium(IV) Complexes of 4-(Furan-2-ylmethyleneamino)benzoic Acid as Catalysts for the Oxidation of Phenol

SUNIL KUMAR[1], PRAVEEN KUMAR GUPTA[1,*] and AMIT KUMAR[2,*]

[1]Department of Chemistry, Maharishi Markandeshwar (Deemed to be University), Mullana-133207, India
[2]Department of Chemistry, Indira Gandhi National College, Ladwa, Kurukshetra-136132, India

*Corresponding authors: E-mail: parveen.gupta@mmumullana.org; amitvash76@gmail.com

Received: 31 July 2026 *Accepted*: 28 October 2026 *Published online*: 13 November 2026 AJC-22541

This study reports the synthesis, characterization and catalytic evaluation of polymer supported Cu(II) and V(IV) complexes for the oxidation of phenol. The heterogeneous catalysts were prepared by covalently immobilizing 4-(furan-2-ylmethyleneamino)benzoic acid onto chloromethylated polystyrene followed by coordination with the respective metal ions. Elemental analysis, spectroscopic characterization and ligand-to-metal stoichiometry confirmed successful complex formation, with metal loadings of 1.40-1.41 mmol g^{-1}. The vanadium complex exhibited square-pyramidal geometry with a V=O bond, while the copper complex having a square-planar geometry. The catalytic activity was evaluated using H_2O_2 and *tert*.-butyl hydroperoxide (TBHP) as oxidants under varying reaction conditions. The Cu(II) catalyst with TBHP achieved a maximum phenol conversion of 94.9% and catechol selectivity of 76.3% under optimized conditions. X-ray diffraction, BET analysis, and thermogravimetric analysis revealed a predominantly amorphous, mesoporous structure with a specific surface area of 54.05 m^2 g^{-1} and thermal stability up to approximately 335 ºC. Spectroscopic analysis confirmed structural stability after repeated catalytic use, while atomic absorption spectroscopy revealed negligible metal leaching over five cycles. These results establish the potential of polymer-supported Cu(II) and V(IV) complexes as reusable heterogeneous catalysts for phenol oxidation.

Keywords: Polymer-supported metal complexes, Chloromethylated polystyrene, Phenol oxidation, Catechol selectivity.

INTRODUCTION

The efficient and selective catalysts are essential for industrial phenol oxidation in fine chemical, pharmaceutical and petrochemical applications. Heterogeneous catalysts offer improved separation and reusability while reducing environmental concerns associated with conventional homogeneous systems [1]. Transition metal complexes are well established as effective catalysts for various oxidation reactions, capable of activating oxidants and facilitating substrate transformations under relatively mild conditions [2]. Nevertheless, their practical utility in homogeneous systems is frequently hindered. Immobilizing these metal complexes onto solid supports offers a promising strategy to overcome these drawbacks, enabling easy separation, recyclability and operational simplicity while preserving high catalytic activity [3-5]. Chloromethylated polystyrene stands out as an attractive polymer support owing to its chemical stability, ease of functionalization and high surface area, making it ideal for anchoring diverse ligands and metal complexes.

Schiff base ligands, especially those derived from heterocyclic moiety, are renowned for their versatile coordination behaviour with transition metals, leading to the formation of stable and catalytically active complexes [6]. In this context, 4-(furan-2-ylmethyleneamino)benzoic acid, possessing both imine, ether and carboxylic acid functionalities, serves as an effective ligand. It forms stable complexes with transition metals and provides reactive sites for covalent immobilization onto polymer support. The present study focuses on the synthesis and catalytic evaluation of anchored Cu(II) and V(II) metal complexes derived from 4-(furan-2-ylmethyleneamino)benzoic acid ligand [7]. Their catalytic activity is subsequently investigated in the oxidation of phenol, yielding catechol and hydroquinone as major products, with other minor products [8,9]. The products of phenol oxidation, catechol and hydroquinone, hold significant industrial and biological importance.

This is an open access journal, and articles are distributed under the terms of the Attribution 4.0 International (CC BY 4.0) License. This license lets others distribute, remix, tweak, and build upon your work, even commercially, as long as they credit the author for the original creation. You must give appropriate credit, provide a link to the license, and indicate if changes were made.

Catechol is an important industrial intermediate used in the manufacture of pesticides, fragrances, pharmaceuticals and dyes. Its strong adhesive properties have attracted interest in the mussel-inspired adhesives, while its derivatives are used as antioxidants and polymer stabilizers [10,11]. Catechol-containing compounds such as dopamine, norepinephrine and epinephrine, play essential roles in neurotransmission and stress regulation. Catechol is further involved in the microbial degradation of organic pollutants [12]. Hydroquinone has traditionally been used as a reducing agent in photographic developers [13,14] and as an antioxidant and stabilizer in plastics, rubber and other polymers [15,16]. It is also a valuable intermediate in the synthesis of pharmaceuticals, agrochemicals, and azo and anthraquinone dyes [17]. These diverse applications underline the importance of developing efficient methods for phenol oxidation. The present study focuses on the synthesis and characterization of reusable polymer-supported metal catalysts for phenol oxidation, with potential applications in other organic transformations, such as hydrogenation, C–C coupling and epoxidation [18,19].

EXPERIMENTAL

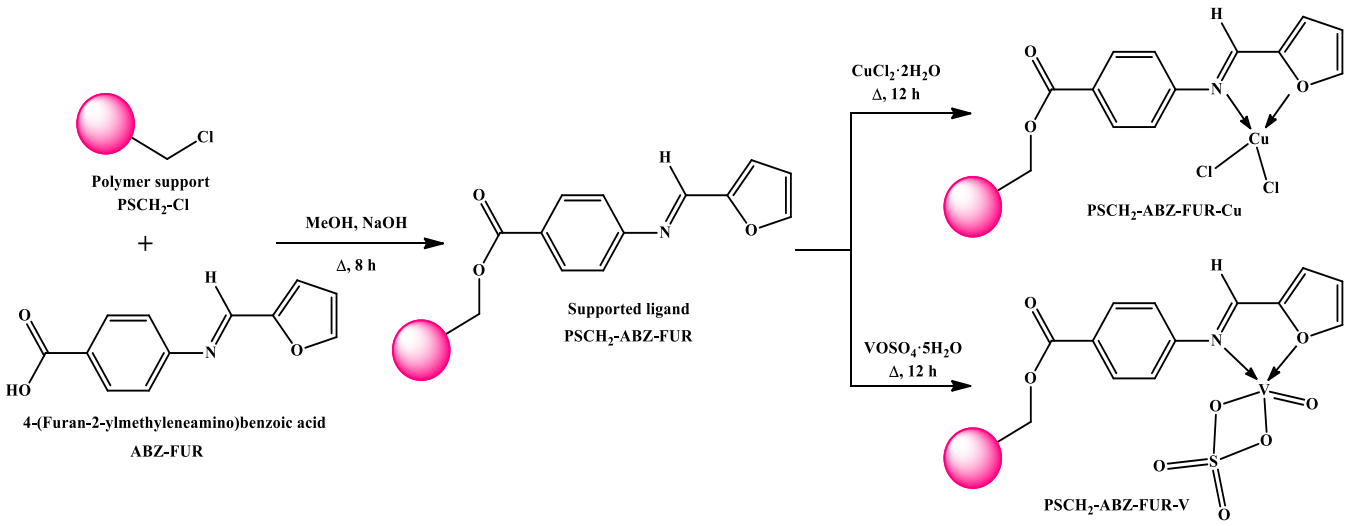
Chloromethylated polystyrene cross-liked with divinylbenzene was obtained from Thermax Chemical Limited Pune, furan-2-carboxyaldehyde (Sigma-Aldrich), vanadyl sulphate pentahydrate, copper chloride, *p*-amino benzoic acid, silver nitrate, conc. HNO_3, H_2O_2 (30%), *tert*-butyl hydroperoxide (TBHP, 70%), methanol, acetonitrile, dimethylformamide sodium hydroxide, and methanol (CDH) were used for the synthesis. All the reagents used were dried and were used without further purification.

FT-IR spectra were recorded on a Shimadzu IR Spirit spectrophotometer, while diffuse reflectance spectra were measured using a Shimadzu UV-2600 spectrophotometer with $BaSO_4$ as the reference. EDX analysis was performed using a Hitachi SU8010 FEG-SEM. Nitrogen analysis was carried out on a Thermo Scientific Flash 2000 analyzer. EPR measurements were obtained using a JES-FA200 spectrometer. Metal content was determined by atomic absorption spectroscopy (Shimadzu ASC-6880) and reaction products were analyzed by GC-MS using an Agilent 7000 GC/TQ system. Thermogravimetric analysis (TGA) was performed using a Mettler Toledo TGA/DSC 3+ SF under an inert atmosphere. BET surface area was measured using a Quantachrome Novatouch LX^4 instrument under N_2 atmosphere and XRD patterns were recorded using a SMARTLAB X-ray diffractometer.

Synthesis of polymer supported 4-(furan-2-ylmethyleneamino)benzoic acid: The chloromethylated polystyrene beads ($PSCH_2$-Cl) (9.0 mmol Cl per gram of resin, 2 g) were pretreated by swelling in 20 mL of methanol for 2 h. A methanolic NaOH solution (9 mmol, 2 g) containing of 4-(furan-2-ylmethyleneamino)benzoic acid [20] was then introduced to the swollen polymer, resulting in an immediate light purple colouration. The mixture was heated to 80 ºC and refluxed with stirring for 8 h (**Scheme-I**). The beads were then washed extensively with hot methanol and hot ethanol, separated by filtration and subsequently dried in an air oven at 80 ºC.

Synthesis of polymer supported metal catalyst: The polymer-supported ligand (0.5 g, 0.225 mmol) was first swelled in 10 mL of DMF for 2 h. Subsequently, a solution of 0.225 mmol of either $CuCl_2{\cdot}2H_2O$ or $VOSO_4{\cdot}5H_2O$ in 15 mL of DMF was introduced to this suspension. The colour of the resin began to alter as the reaction proceeded. After cooling, the solid beads were collected *via* filtration, washed thoroughly with hot DMF, methanol and ethanol and finally dried in oven at 80º C (**Scheme-I**).

Catalytic oxidation reaction: The catalytic oxidation of phenol was carried out in a round-bottom flask maintained at the desired temperature. The catalyst was pre-swollen in 20 mL of acetonitrile for 1 h, followed by the addition of phenol (10 mmol), selected oxidant (10 mmol; TBHP or H_2O_2) and catalyst (0.1 or 0.15 g). Reaction progress was monitored by thin-layer chromatography (TLC). The effects of catalyst loading, oxidant type, reaction temperature and reaction time (3-7 h) were systematically evaluated to optimize the reaction conditions. After completion, the catalyst was recovered by filtration, washed several times with hot solvent and the reaction products were analyzed by GC-MS.



Scheme-I: Synthesis of polymer-supported metal catalyst of 4-(furan-2-ylmethyleneamino)benzoic acid

RESULTS AND DISCUSSION

The cross-linked chloromethylated polystyrene was functionalized with 4-(furan-2-ylmethyleneamino)benzoic acid [20] using DMF as solvent, resulting in the formation of the polymer-supported ligand [PSCH$_2$-ABZ-FUR] (**Scheme-I**). The successful attachment of the ligand to the polymer matrix was initially verified by heating the PSCH$_2$-ABZ-FUR beads with pyridine at 100 ºC for 3 h followed by treatment with conc. HNO_3 and $AgNO_3$ solution. The absence of a white precipitate confirmed the complete substitution of the chloromethyl groups by the ligand. The functionalized polymer, bearing ligands at the *para* position of the phenyl rings in the polymer backbone, is depicted in Fig. 1. The coordination of metal salts with the functionalized beads to generate polymer supported metal catalysts was preliminarily evidenced by a distinct colour change of the beads. The analytical data for the polymer-supported ligand and its metal complexes are shown in Table-1.

EDX analysis: The loading of the ligand and the incorporation of the metal ion into the polymer support were also confirmed through EDX analysis (Fig. 2). The polymer supported ligand [PSCH$_2$-ABZ-FUR] exhibits only C, O and N signals, which confirm the anchoring of the ligand to the polymer. The presence of metal signal in all complexes shows the attachment of the respective metal ions to [PSCH$_2$-ABZ-FUR]. The EDX spectrum of the Cu catalyst shows a Cl signal, whereas the V catalyst exhibits an S signal. These signals may indicate the presence of residual chlorine- and sulphur containing species.

FT-IR study: Fig. 3 illustrates the FT-IR spectra of the compounds, presented both individually and in a stacked arrangement. Table-2 compiles the significant IR bands for the [PSCH$_2$-ABZ-FUR] ligand and its metal(II) complexes. The FTIR spectrum of [PSCH$_2$-ABZ-FUR] exhibits characteristic bands at 1731, 1630 cm^{-1} and 1254, 1075 cm^{-1}, assigned

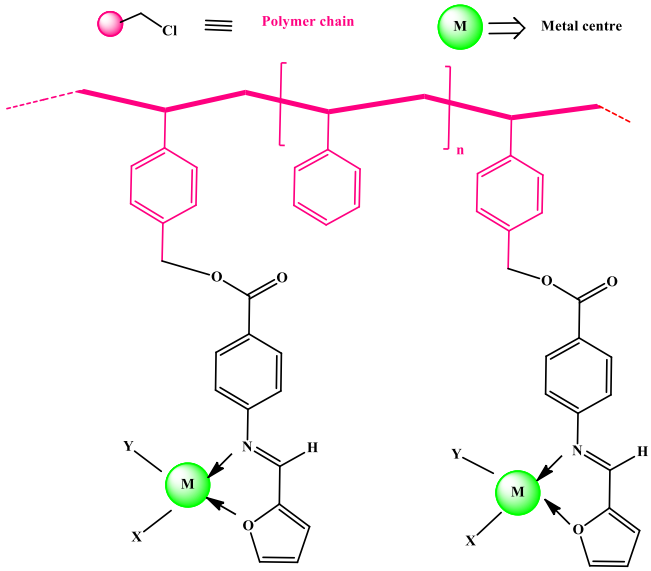


Fig. 1. Functionalized chloromethylated polystyrene beads (neglecting the cross-linking with divinylbenzene)

to ν(C=O), ν(C=N) and asymmetric and symmetric furan ν_{asy}(C-O-C)/ν_{sy}(C-O-C) stretching vibrations, respectively. The comparison of the ligand and metal-complex spectra reveals a 20-22 cm^{-1} shift in the C=N stretching band, which confirm the coordination through the azomethine nitrogen. Shifts of 10-19 cm^{-1} in the furan C–O–C stretching bands further suggest the involvement of oxygen in metal coordination [21]. Additional bands at 485-481 and 575-570 cm^{-1} are assigned to M–N and M–O vibrations, respectively, while the band at 365 cm^{-1} is attributed to M–Cl stretching. The vanadium complex exhibits a characteristic ν(V=O) stretching band at 975 cm^{-1} [22]. Bands at 1148 and 1055 cm^{-1} are assigned to asymmetric and symmetric S–O stretching vibrations respectively, which confirm the presence of coordinated

TABLE-1
ANALYTICAL DATA OF PSCH$_2$-ABZ-FUR AND ITS METAL CATALYST

Compound	Colour	Elemental analysis (%)		Ligand incorporation (mmol per gram of resin)	Metal incorporation (mmol per gram of resin)	Ligand:Metal ratio
		N	M			
[PSCH$_2$-ABZ-FUR]	Off white	3.2	–	2.28	–	–
[PSCH$_2$-ABZ-FUR-V]	Light brown	2.1	7.2	1.50	1.41	1.06:1
[PSCH$_2$-ABZ-FUR-Cu]	Brown	2.4	8.9	1.71	1.40	1.21:1

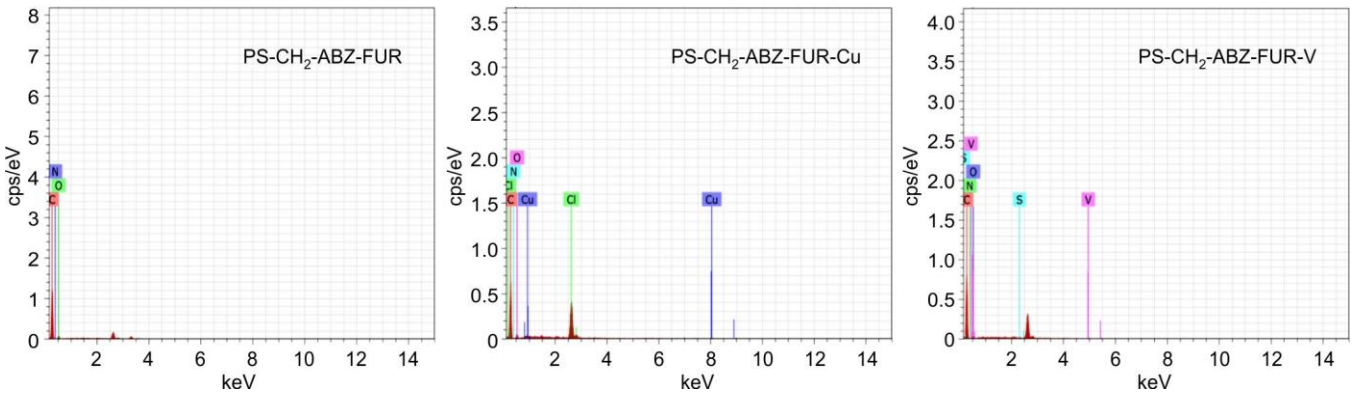


Fig. 2. EDX plot of [PSCH$_2$-ABZ-FUR], [PSCH$_2$-ABZ-FUR-Cu] and [PSCH$_2$- ABZ-FUR-V]

TABLE-2
FTIR DATA (cm^{-1}) FOR THE $PSCH_2$-ABZ-FUR AND ITS METAL COMPLEXES

Polymer-supported compounds	ν(C=N)	ν_{asy}(C-O-C)/ ν_{sy}(C-O-C)	$\nu_{sy}(SO_4)$/ $\nu_{asy}(SO_4)$	ν(V=O)	ν(M-N)	ν(M-O)	ν(M-Cl)
[$PSCH_2$-ABZ-FUR]	1630	1254/1075	–	–	–	–	–
[$PSCH_2$-ABZ-FUR-V]	1610	1264/1094	1148, 1055	975	485	570	–
[$PSCH_2$-ABZ-FUR-Cu]	1608	1264/1082	–	–	481	575	365

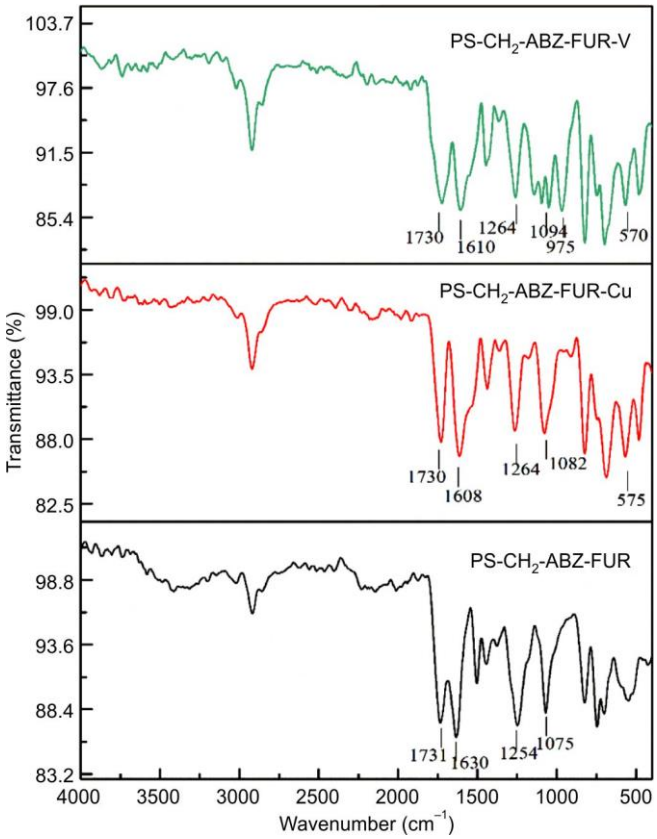


Fig. 3. FT-IR spectra of functionalized polymer and polymer supported metal catalysts

sulphate groups [$\nu_{asy}(SO_4)$ and $\nu_{sy}(SO_4)$] [23]. These spectral changes support metal coordination with the polymer supported ligand.

Diffused reflectance spectra: Fig. 4 shows the individual and overlaid reflectance spectra of the polymer supported metal complexes, which reflects their electronic transitions and coordination environments (Table-3). The uncomplexed [$PSCH_2$-ABZ-FUR] ligand exhibits absorption bands at 38,023 and 28,490 cm^{-1}, assigned to π→π* and n→π* transitions, respectively. These bands shift slightly upon metal coordination, suggesting changes in the electronic environment of ligand. The vanadium(IV) complex exhibits three *d*–*d* transitions at 12,004, 16,000 and 23,255 cm^{-1}, assigned to the

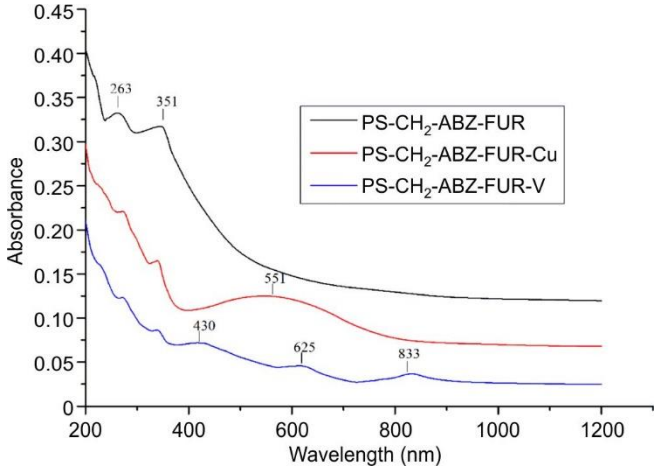


Fig. 4. Overlay and individual DRS spectra of polymer supported metal catalysts

$^2B_2 \rightarrow {}^2E$ ($d_{xy} \rightarrow d_{xz;yz}$), $^2B_2 \rightarrow {}^2B_1$ ($d_{xy} \rightarrow d_{x^2-y^2}$) and $^2B_2 \rightarrow {}^2A_1$ ($d_{xy} \rightarrow d_{z^2}$) transitions, respectively [24]. These transitions are consistent with a five-coordinate oxovanadium(IV) centre with approximate C_{4V} symmetry and support the proposed square-pyramidal geometry. The copper(II) complex displays a broad absorption band centred at approximately 18,148 cm^{-1}, which may comprise overlapping $^2B_{1g} \rightarrow {}^2A_{1g}$; $^2B_{1g} \rightarrow {}^2B_{2g}$; $^2B_{1g} \rightarrow {}^2E_g$ transitions [25]. This broad spectral feature is consistent with a square-planar (D_{4h}) copper(II) coordination environment.

EPR study: The X-band EPR spectrum of the [$PSCH_2$-ABZ-FUR-V] complex recorded at 9.45 GHz exhibits a well-resolved eight-line hyperfine pattern characteristic of a V^{IV} (d^1) system (Fig. 5). The observed hyperfine splitting arises from the interaction of the unpaired electron (S = 1/2) with the ^{51}V nucleus (I = 7/2). This interaction gives rise to eight hyperfine lines in accordance with the 2I+1 rule and confirms the presence of VO^{2+} species. The spectrum exhibits marked anisotropy with $g_{\|}$ = 2.01 and $g_{\perp}$ =2.21. The hyperfine coupling constants are $A_{\perp}$ =178 G and $A_{\|}$ =81 G. These parameters are characteristic of an axially symmetric vanadium centre. The observed g-value anisotropy supports the assignment of a d_{xy} ground state which is commonly associated with oxovanadium(IV) complexes [26]. The strong hyperfine interaction further supports significant metal-ligand covalency

TABLE-3
DIFFUSED REFLECTANCE SPECTRAL DATA OF POLYMER SUPPORTED METAL CATALYSTS

Supported metal catalysts	Band position (cm^{-1})	Band assignment
[$PSCH_2$-ABZ-FUR]	38023; 28490	π→π*; n→π*
[$PSCH_2$-ABZ-FUR-V]	12004; 16000; 23255	$^2B_2 \rightarrow {}^2E$; $^2B_1$; $^2A_1$
[$PSCH_2$-ABZ-FUR-Cu]	18148	$^2B_{1g} \rightarrow {}^2A_{1g}$; $^2B_{2g}$; ^2E_g

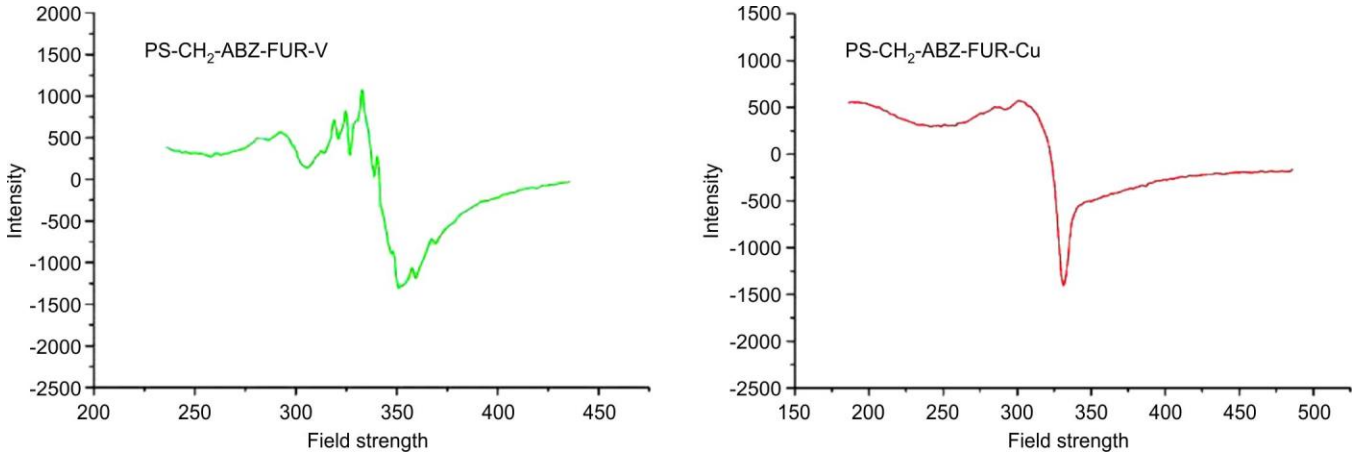
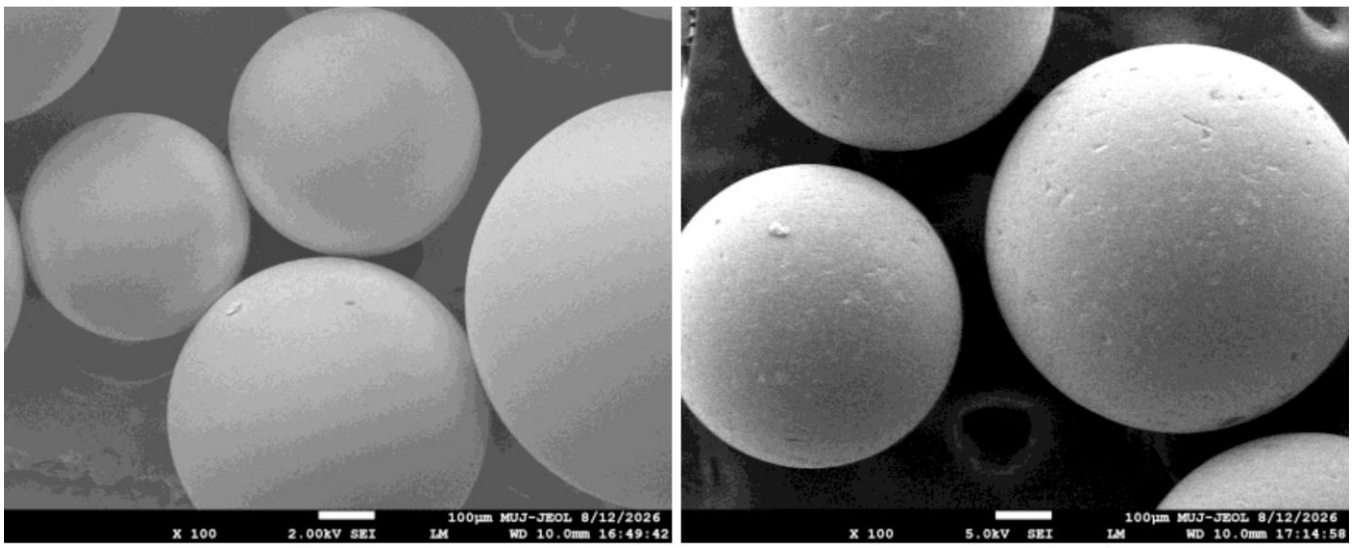


Fig. 5. EPR plots of [PSCH$_2$-ABZ-FUR-V] and [PSCH$_2$-ABZ-FUR-Cu]

and the presence of a short V=O bond. The spectral features are consistent with a square pyramidal geometry, wherein the oxo group occupies the axial position and the equatorial plane is coordinated by donor atoms from the ligand framework. The absence of zero-field splitting is consistent with an S = 1/2 system. The EPR parameters support the assignment of a mononuclear V(IV) centre in an axially distorted coordination environment characteristic of oxovanadium(IV) complexes. The room-temperature X-band EPR spectrum of [PSCH$_2$-ABZ-FUR-Cu] exhibits a broad anisotropic resonance (Fig. 5). The observed g-values ($g_{\|}$ = 2.32 and $g_{\perp}$ =2.08) are consistent with an axially distorted coordination environment around the Cu(II) ion. These values support a $d_{x^2-y^2}$ ground-state assignment [27]. The hyperfine lines split $g_{\|}$ signals with an average spacing of 155G. Such a ground state is characteristic of square planar geometry arising from Jahn-Teller distortion in Cu(II) complexes. The g-value exceeds the free-electron value of 2.0023 and points to an appreciable orbital contribution and spin–orbit coupling typical of Cu(II) (d^9) systems. The S = 1/2 configuration of Cu(II) precludes zero-field splitting. The observed spectral anisotropy arises primarily from g-tensor anisotropy. The EPR results support the presence of paramagnetic Cu(II) species in a distorted axial coordination environment.

SEM analysis: SEM was performed to characterize the morphology of [PSCH$_2$-ABZ-FUR] and [PSCH$_2$-ABZ-FUR-Cu] as shown in Fig. 6. It was found that [PSCH$_2$-ABZ-FUR] has uniform and smooth surface whereas after the binding of copper, the surface is slightly rough. This shows a regular spreading of metal particles and effective catalyst preparation.

BET analysis: BET surface area analysis was used to evaluate the specific surface area and pore volume of the Cu catalyst by using N_2 adsorption/desorption measurements at 77.35 K. The nitrogen adsorption/desorption isotherms of copper catalyst are shown in Fig. 7. According to the results, BET surface area 54.045 $m^2\ g^{-1}$ and a total pore volume is 0.3089 $cm^3\ g^{-1}$ respectively. The BET-derived average pore diameter is 11.433 nm, while the BJH analysis yielded an average pore diameter of 6.7263 nm. Both values lie within the mesoporous range of 2-50 nm and confirm the mesoporous character of the copper-bound polystyrene-supported



PS-CH$_2$-ABZ-FUR PS-CH$_2$-ABZ-FUR-Cu

Fig. 6. SEM micrographs of [PSCH$_2$-ABZ-FUR] and [PSCH$_2$-ABZ-FUR-Cu]

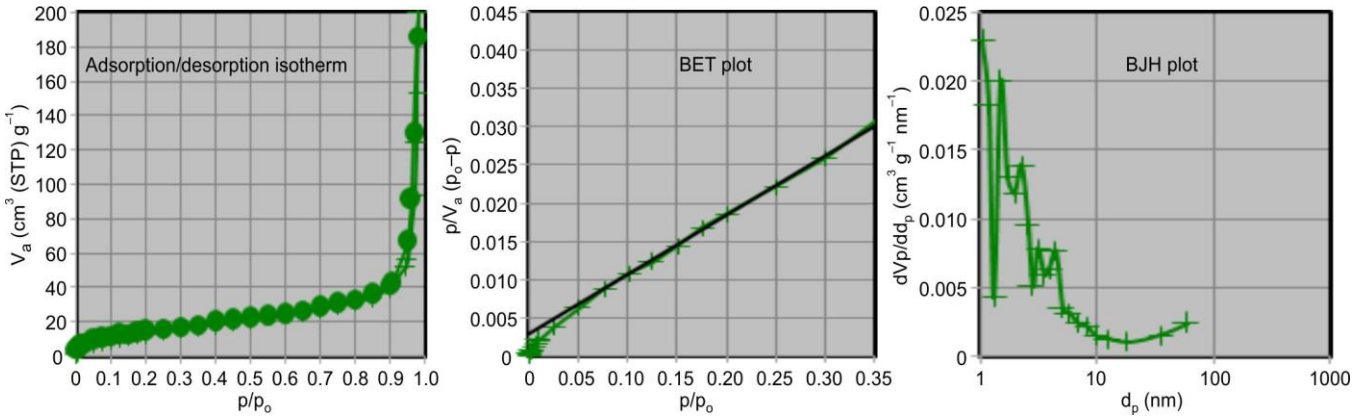


Fig. 7. N_2 adsorption-desorption isotherm, BET surface area plot and BJH pore-size distribution of the [PSCH$_2$-ABZ-FUR-Cu]

ligand. BJH analysis yielded a pore volume of 0.1589 cm^3 g^{-1} and a median pore diameter of 24.386 nm. These values point to a broad and heterogeneous pore-size distribution. The results establish that the copper catalyst has appreciable surface area and pore volume with predominantly mesoporous characteristics.

Power XRD analysis: The copper catalyst exhibits broad XRD peaks at 2θ values between 10° and 30° which are characteristic of the amorphous polystyrene structure. A broad peak near 40° appears after copper coordination with the polystyrene-supported ligand. The absence of sharp diffraction peaks associated with nanocrystalline CuO suggests that crystalline CuO phases are not detectable following metal incorporation [28,29] (Fig. 8).

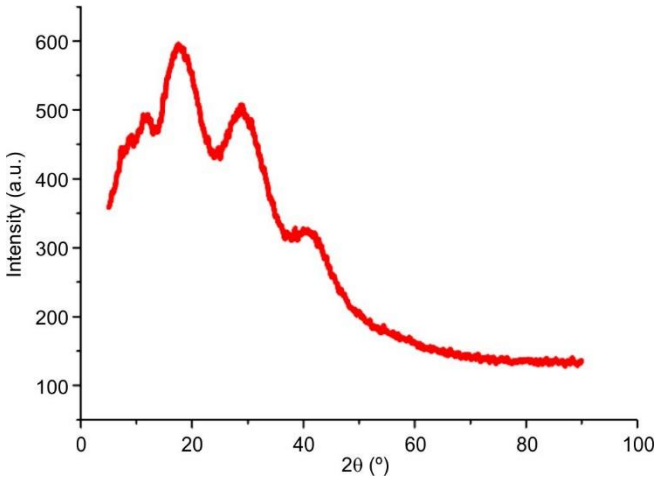


Fig. 8. XRD pattern of [PSCH$_2$-ABZ-FUR-Cu]

TGA analysis: The thermal stability of the polystyrene-supported copper complex was investigated by thermogravimetric analysis. The TGA curve (Fig. 9) shows a major weight-loss between 335.52 to 442.33 ºC, which represents approximately 57.4% of the initial sample mass of 3.20 mg. This major weight loss is attributed predominantly to the thermal degradation of the organic polymer supported ligand framework. A further weight loss of approximately 8.7% was observed between 613.67 and 621.96 ºC, which may be associated with the degradation of residual organic or carbonaceous species. The TGA profile confirms the catalyst's

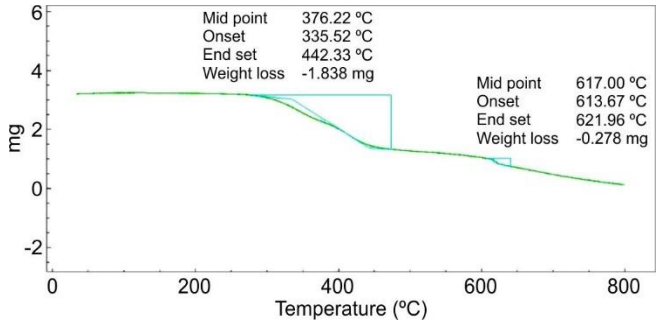


Fig. 9. Thermogram of copper-bound polystyrene-supported ligand

thermal stability under the employed reaction conditions. The onset of major decomposition occurs at approximately 335 ºC which is well above the reaction temperature of 65 ºC.

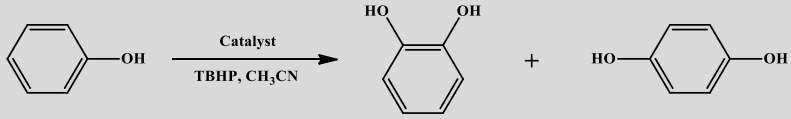
Catalytic activity: The catalytic activity of the synthesized polymer-supported V(IV) and Cu(II) catalysts was evaluated through phenol oxidation. Catechol and hydroquinone were identified as the major products along with minor unidentified products. The effects of oxidant type and concentration as well as reaction time, temperature and catalyst dosage were examined to establish suitable conditions for improving product yield and oxidation efficiency.

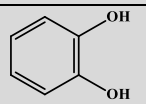
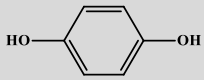
Effect of oxidant: The effects of TBHP and H_2O_2 on phenol oxidation were examined to identify the most effective oxidant. No reaction occurred in the absence of an oxidant. Tables 4 and 5 establish TBHP in acetonitrile as the more effective system for phenol oxidation. Hydrogen peroxide gave a lower conversion under the tested conditions.

Effect of reaction temperature: Reaction temperature played a key role in phenol oxidation over the synthesized catalysts. Experiments were conducted at 40-80 ºC for 8 h using a 1:1 mmol ratio of phenol to TBHP or H_2O_2 in acetonitrile. Phenol conversion increased with rising temperature while negligible conversion occurred below 40 ºC (Tables 4 and 5). At higher temperatures the rapid decomposition of the peroxide oxidant reduced the overall conversion. A temperature of 65 ºC was found to be optimal for efficient phenol oxidation.

Effect of reaction time: The Phenol oxidation was monitored using TBHP and H_2O_2 at a 1:1 ratio with catalyst loadings of 0.1 and 0.15 g under continuous stirring at different temperatures. Negligible conversion occurred during the

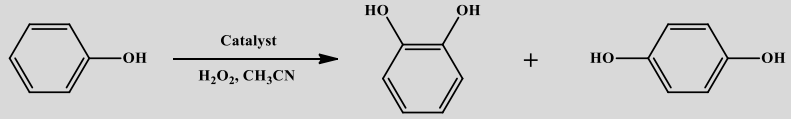
TABLE-4
EFFECT OF CATALYST CONCENTRATION AND REACTION TIME ON PHENOL CONVERSION AND PRODUCT SELECTIVITY USING DIFFERENT CATALYSTS

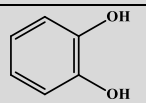
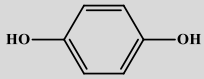


Compound	Catalyst concentration (g)	Time (h)	Conversion (%)	Selectivity (%)		
						Others
Blank/Polymer alone		3	2.2	59.2	8.6	32.2
		4	7.9	59.9	10.7	29.4
		5	8.3	60.8	10.9	28.3
		6	9.3	60.8	10.9	28.3
[PSCH$_2$-ABZ-FUR-Cu]	0.1	3	26.3	70.3	27.9	1.8
		4	86.4	71.8	26.5	1.7
		5	90.7	74.5	23.6	1.9
		6	93.1	74.5	24.9	1.6
	0.15	3	29.1	71.1	27.7	1.2
		4	87.3	72.7	27.5	0.8
		5	91.9	76.3	23.4	0.3
		6	94.9	76.3	23.4	0.3
[PSCH$_2$-ABZ-FUR-V]	0.1	3	16.8	58.9	40.6	0.5
		4	59.2	60.7	37.8	1.5
		5	61.8	65.7	34.0	0.3
		6	63.4	65.7	34.0	0.3
	0.15	3	18.7	59.9	38.6	1.5
		4	61.3	62.8	36.9	0.3
		5	64.6	66.9	32.5	0.6
		6	65.9	66.9	32.5	0.6

*Reaction conditions: CH_3CN (20 mL), phenol (10 mmol), TBHP (10 mmol), temperature (65 ºC); conversion refers to GCMS analysis.

TABLE-5
EFFECT OF CATALYST CONCENTRATION AND REACTION TIME ON PHENOL CONVERSION AND PRODUCT SELECTIVITY USING DIFFERENT CATALYSTS



Compound	Catalyst concentration (g)	Time (h)	Conversion (%)	Selectivity (%)		
						Others
Blank/Polymer alone		3	2.1	57.7	10.7	31.6
		4	6.8	58.9	10.4	30.7
		5	8.3	59.6	11.8	28.6
		6	9.4	59.7	11.7	28.6
[PSCH$_2$-ABZ-FUR-Cu]	0.1	3	21.3	68.4	29.8	1.8
		4	83.6	68.3	30.0	1.7
		5	89.8	69.6	28.8	1.6
		6	92.2	70.5	28.0	1.5
	0.15	3	23.4	68.4	29.8	1.8
		4	87.3	69.5	29.8	0.7
		5	91.6	70.3	28.2	1.5
		6	93.8	70.9	28.7	0.4
[PSCH$_2$-ABZ-FUR-V]	0.1	3	17.8	55.5	43.3	1.2
		4	56.4	56.3	42.5	1.2
		5	58.9	57.6	41.6	0.8
		6	61.5	57.7	41.3	1.0
	0.15	3	18.2	56.2	42.5	1.3
		4	57.3	56.8	41.8	1.4
		5	59.8	59.9	39.3	0.8
		6	63.6	60.1	39.1	0.8

*Reaction conditions: CH_3CN (20 mL), phenol (10 mmol), H_2O_2 (10 mmol), temperature (65 ºC); conversion refers to GCMS analysis.

first 2 h which points to an induction period. Phenol conversion then increased with reaction time for all catalysts. As shown in Fig. 10, the highest conversion was attained after 6 h and remained nearly constant thereafter. Product selectivity showed little variation with reaction time, which indicates that extending the reaction beyond 6 h offers no substantial improvement in product distribution.

Effect of amount of catalyst: The effect of catalyst loading on phenol oxidation was examined using 0.1 and 0.15 g of catalyst at 65 ºC for 3-7 h while maintaining a 1:1 ratio of phenol to TBHP or H_2O_2. The control experiments conducted without the catalyst or with the polymer alone gave very low phenol conversion of approximately 9.3-9.4% in the presence of either oxidant. A catalyst loading of 0.1 g gave moderate conversion while increasing the amount to 0.15 g improved conversion through the availability of more active sites for substrate–oxidant interaction (Tables 4 and 5). Further increases in catalyst loading did not significantly improve conversion which points to a limit beyond which additional catalyst offers little benefit.

Hot filtration test: The heterogeneous nature of the catalytic system was examined by a hot filtration test. The polymer-supported catalyst was removed from the reaction mixture after 30 min under the optimized conditions. No further phenol conversion occurred in the filtrate. This result supports the role of the immobilized metal catalyst in the oxidation process and suggests that leached metal species do not contribute significantly to the catalytic activity.

Catalyst reusability: The reusability of the polymer-supported metal catalysts was evaluated through successive phenol oxidation cycles. After each run the catalyst was recovered by filtration and washed and dried before reuse under the optimized conditions. The products retained similar characteristics and yields during the initial cycles. As shown in Fig. 11, phenol conversion gradually declined after five cycles while product selectivity remained nearly unchanged. IR and DRS analyses of the recovered catalysts revealed no significant spectral changes after repeated use. However, AAS measurements revealed a slight decrease in metal content after five cycles. These results support the structural stability

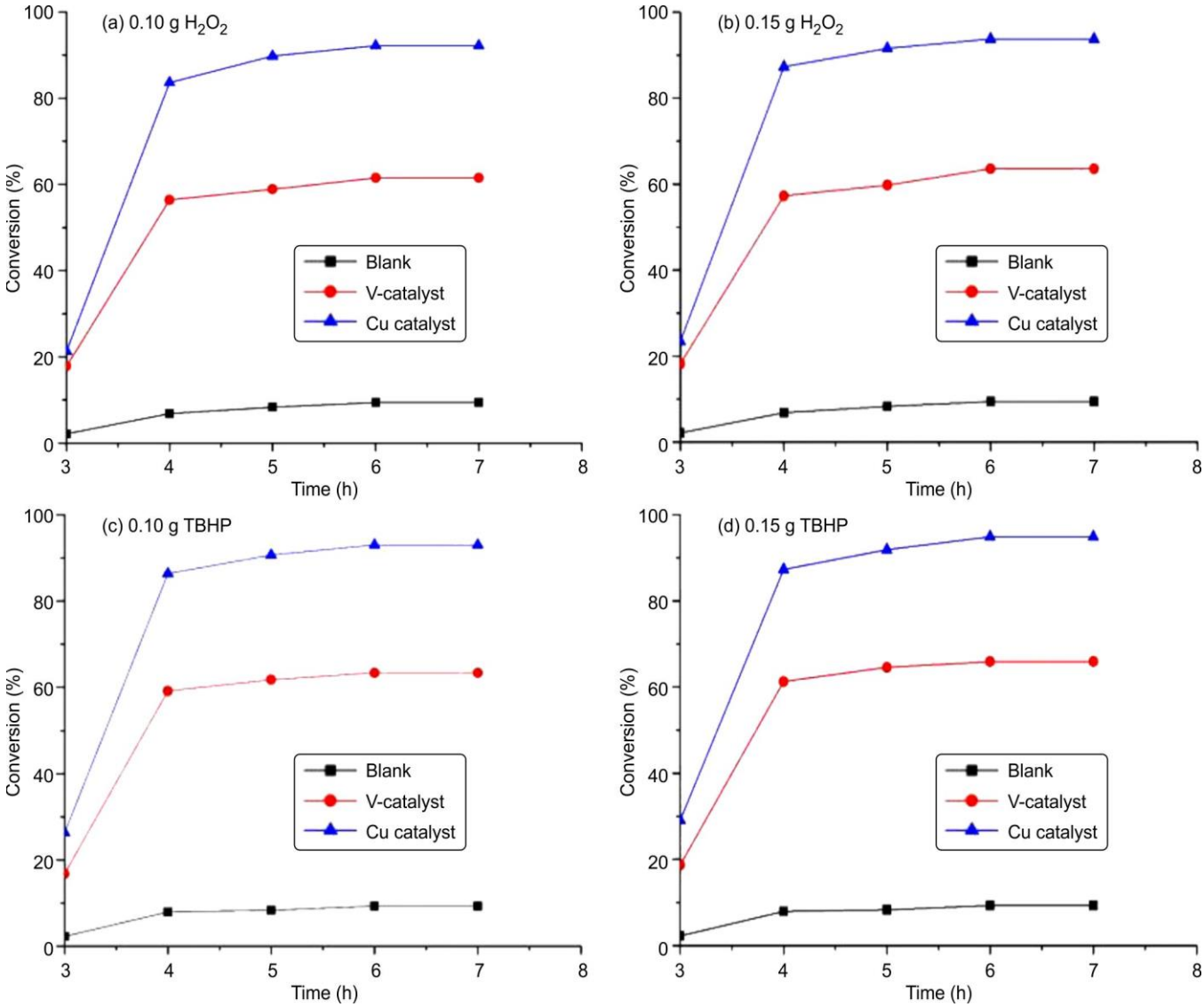


Fig. 10. Plots of time variation on Phenol oxidation with polystyrene-anchored catalysts

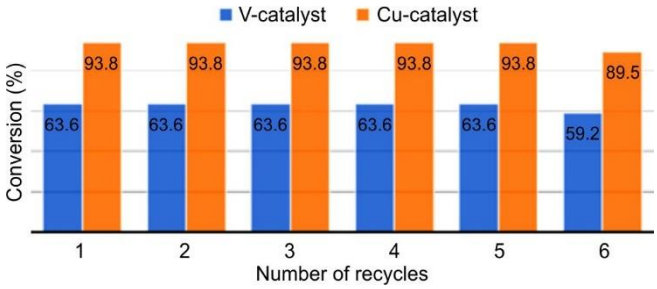


Fig. 11. Comparison of phenol conversion efficiency of V-catalyst and Cu-catalyst over six consecutive reaction cycles

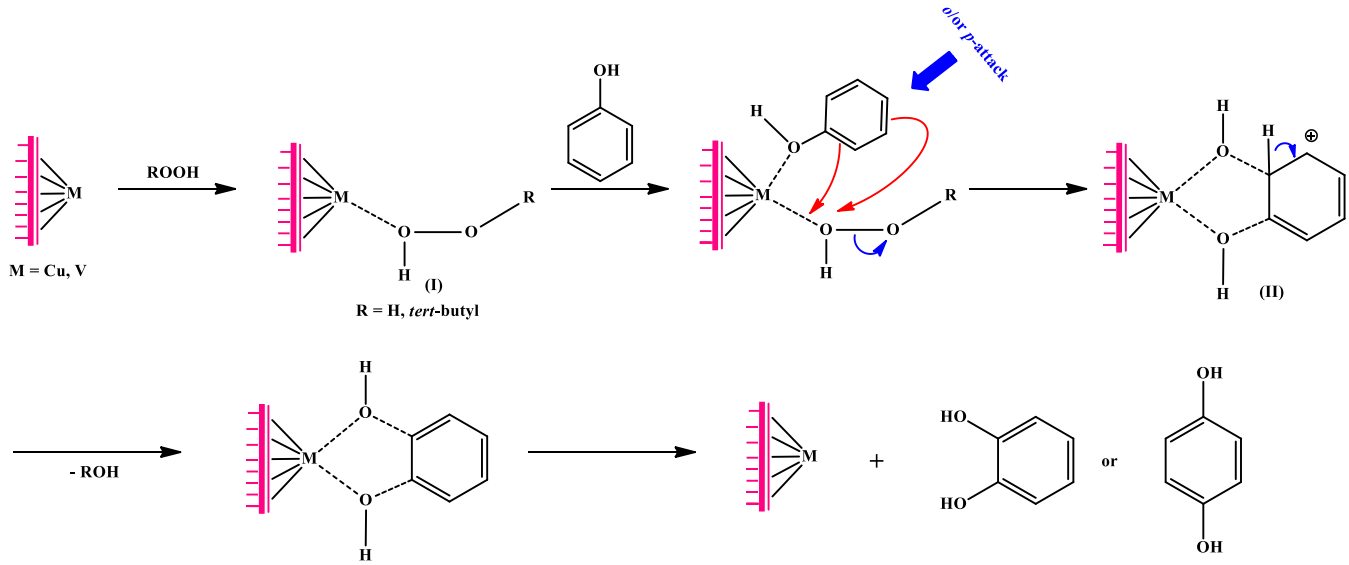
and reusability of the catalysts with only a minor loss of catalytic activity over successive cycles.

Plausible mechanism: A mechanistic pathway for the polymer-supported metal-catalyzed oxidation of phenol by peroxides (H_2O_2/TBHP) is shown in **Scheme-II**. The initial step involves the coordination of the peroxide to the metal centre, forming a peroxo-metal complex (**I**) [30]. Subsequently, phenol also coordinates to the catalyst. The O–O bond of the oxidant becomes polarized and activated, which facilitate oxygen atom transfer to the *ortho* or *para* position of the phenol ring *via* a transition state. This yields a hydroxycyclohexadienone-type intermediate (II). Electron reorganization within this intermediate then leads to the formation of catechol (from *ortho* substitution) or hydroquinone (from *para* substitution). Regeneration of the metal catalyst, often accompanied by the release of water or *tert.*-butanol as a byproduct found in GC-MS studies.

Comparative studies: The synthesized polymer-supported metal catalysts were also compared with reported systems for phenol oxidation. Table-6 highlights the promising performance of the Cu catalyst, which achieved high phenol conversion and catechol selectivity under relatively mild reaction conditions.

Conclusion

This study reports the synthesis and catalytic application of polymer-supported 4-(furan-2-ylmethyleneamino)benzoic acid complexes containing Cu(II) and V(IV). The ligand was



Scheme-II: Proposed mechanism for the H_2O_2/TBHP mediated oxidation of phenol catalyzed by supported metal catalyst

TABLE-6
COMPARISON DATA OF PRESENT CATALYSTS AND REPORTED CATALYTIC SYSTEMS

Catalyst	Reaction condition oxidant/solvent/temp/time	Conversion (%)	Selectivity (%)	Ref.
[$Mo^{VI}O_2${Hdfba(fah)$_2$}(H_2O)]@ APTMS-TiO_2; [$Mo^{VI}O_2${Hdfba(bhz)$_2$}(H_2O)]@ APTMS-TiO_2	H_2O_2/CH_3CN/80 ºC/6 h	100	94	[31]
3MHBdMBn-M complexes [M = Fe(III), Co(II), Ni(II), Cu(II) and Zn(II) ions]	H_2O_2/CH_3CN/70 ºC/ 1440 min	50.5	96.5	[32]
Non-PS & PS-HPHZ-M [*N,N-bis*-(*o*-hydroxyacetophenone)-hydrazine] Fe(III), Cu(II) and Zn(II)	H_2O_2/CH_3CN/70 ºC, 24 h	31-56 36-62	78-86 86.1-90.5	[33]
MOBdMBn-Zn-*N,N'-bis*(2-hydroxy-3-methoxybenzaldehyde)4-methylbenzene-1,2-diamine	H_2O_2/CH_3CN/70 ºC, 4 h	25.9	89.4	[34]
PS-HIMAP-Cu[Polymer-supported Cu(II) complex of 2-((1*H*-indole-3-yl)methyleneamino)phenol]	TBHP/CH_3CN/70 ºC/6 h	97.2	91.5	[35]
Zirconium phosphate supported Cu(II) catalyst	O_2/CH_3CN/30 ºC, 2 h	66	60	[36]
VO-(EtOsalphen)[3-ethoxy salicylaldehyde-1,2-diaminobenzene]; VO-(EtOsalnaph)[3-ethoxysalicylaldehyde-1,8-diaminonaphthalene]	H_2O_2/CH_3CN/70 ºC, 6 h	71 76.6	92.5 94.2	[37]
[PSCH$_2$-4-(furan-2-ylmethyleneamino)benzoic acid-Cu]	TBHP/CH_3CN/65 ºC/6 h	94.9	76.3	Present work
[PSCH$_2$-4-(furan-2-ylmethyleneamino)benzoic acid-Cu]		65.9	66.9	

anchored onto chloromethylated polystyrene before metal incorporation. Under optimized conditions (0.15 g catalyst at 65 ºC for 6 h) the catalysts promoted phenol oxidation using H_2O_2 or TBHP. The Cu(II) catalyst exhibited the highest conversion (94.9%) and selectivity (76.3%) with TBHP. The V(IV) catalyst showed lower conversion (65.9%) and selectivity (66.9%) under the same oxidant conditions. Increasing the catalyst loading improved conversion up to 0.15 g beyond, which further improvement was limited. Recycling tests showed that catalytic performance and product selectivity were largely retained over five cycles. AAS and spectroscopic analyses revealed only minor metal loss and no significant structural changes. A plausible mechanism involving a metal–peroxo complex and hydroxycyclohexadienone-type intermediates is proposed.

ACKNOWLEDGEMENTS

The authors are thankful to the Maharishi Markandeshwar (Deemed to be University), Mullana, India

CONFLICT OF INTEREST

The authors declare that there is no conflicts of interest regarding the publication of this article.

DECLARATION OF AI-ASSISTED TECHNOLOGIES

During the preparation of this manuscript, the authors used an AI-assisted tool(s) to improve the language and no data, results or scientific conclusions were generated by AI. All analyses, interpretations and conclusions are the authors' own. The authors reviewed and edited the content and take full responsibility for the published work.

REFERENCES

1. B. Bouzayani and M.Á. Sanromán, *Molecules*, **29**, 2188 (2024); https://doi.org/10.3390/molecules29102188
2. T. Punniyamurthy, S. Velusamy and J. Iqbal, *Chem. Rev.*, **105**, 2329 (2005); https://doi.org/10.1021/cr050523v
3. S. Moulay, *Polym. Plast. Technol. Eng.*, **57**, 1045 (2018); https://doi.org/10.1080/03602559.2017.1370109
4. P. Mastrorilli and C.F. Nobile, *Coord. Chem. Rev.*, **248**, 377 (2004); https://doi.org/10.1016/j.ccr.2004.02.003
5. C.H. Raksha, M.P. Yogeesh and N.S. Shetty, *Discov. Appl. Sci.*, **7**, 565 (2025); https://doi.org/10.1007/s42452-025-07106-x
6. Y. Gong, X. Cao, M. Zhao, Y. Xu and Y. Geng, *Mol. Cryst. Liq. Cryst. (Phila. Pa.)*, **765**, 54 (2023); https://doi.org/10.1080/15421406.2023.2213583
7. S.A. Kazmi, I.H. Shah, M. Fatima, A. Amer, A. Ghaffar, A. Shaheen, N. Tariq, S. Shaheen and A. Ahmad, *Sch. J. Eng. Technol*, **13**, 492 (2025); https://doi.org/10.36347/sjet.2025.v13i07.005
8. M.A. Bashir, J. Wei, H. Wang, F. Zhong and H. Zhai, *Org. Chem. Front.*, **9**, 5395 (2022); https://doi.org/10.1039/D2QO00758D
9. M.R. Maurya, S.J. Titinchi, S. Chand and I.M. Mishra, *J. Mol. Catal. Chem.*, **180**, 201 (2002); https://doi.org/10.1016/S1381-1169(01)00435-6
10. S. Razaviamri, K. Wang, B. Liu and B.P. Lee, *Molecules*, **26**, 559 (2021); https://doi.org/10.3390/molecules26030559
11. S. Suresh, V.C. Srivastava and I.M. Mishra, *Int. J. Energy Environ. Eng.*, **3**, 32 (2012); https://doi.org/10.1186/2251-6832-3-32
12. D.T. Gibson, *Science*, **161**, 1093 (1968); https://doi.org/10.1126/science.161.3846.1093
13. P.D. Banodkar and K.P. Banodkar, *Indian J. Dermatol. Venereol. Leprol.*, **88**, 696 (2022); https://doi.org/10.25259/IJDVL_657_2021
14. F.J. Enguita and A.L. Leitão, *Scient. World J.*, 2013, 542168 (2013); https://doi.org/10.1155/2013/542168
15. R. Pfaendner, *Macromol. Mater. Eng.*, **310**, 2500039 (2025); https://doi.org/10.1002/mame.202500039
16. D. Pavlovskyi and V. Vorobyova, *Clean Technol. Environ. Policy*, **28**, 80 (2026); https://doi.org/10.1007/s10098-026-03415-w
17. A. Valenzuela, D. Ballestero, C. Gan, G. Lorca, E. Langa and M.R. Pino-Otín, *Toxics*, **12**, 115 (2024); https://doi.org/10.3390/toxics12020115
18. A. Santos, P. Yustos, S. Rodriguez and F. Garcia-Ochoa, *Appl. Catal. B*, **65**, 269 (2006); https://doi.org/10.1016/j.apcatb.2006.02.005
19. J. Wu and M.C. Kozlowski, *ACS Catal.*, **12**, 6532 (2022); https://doi.org/10.1021/acscatal.2c00318
20. J. Parekh, P. Inamdhar, R. Nair, S. Baluja and S. Chanda, *J. Serb. Chem. Soc.*, **70**, 1155 (2005); https://doi.org/10.2298/JSC0510155P
21. N.M. Hosny, G. Samir and M.H. Abdel-Rhman, *BMC Chem.*, **18**, 22 (2024); https://doi.org/10.1186/s13065-023-01098-8
22. B.S. Far, G. Grivani, A.D. Khalaji, M. Khorshidi and A. Gholizadeh, *J. Mol. Struct.*, **1197**, 361 (2019); https://doi.org/10.1016/j.molstruc.2019.07.055
23. F. Ucun and A. Tokatlı, *Iran. J. Chem. Chem. Eng*, **40**, 881 (2021); https://doi.org/10.30492/ijcce.2020.38180
24. X. Gao and I.E. Wachs, *J. Phys. Chem. B*, **104**, 1261 (2000); https://doi.org/10.1021/jp992867t
25. J.D. Chellaian and S.S. Raj, *J. Heterocycl. Chem.*, **58**, 928 (2021); https://doi.org/10.1002/jhet.4209
26. A. Mondal, S. Sarkar, D. Chopra, T.N. Guru Row, K. Pramanik and K.K. Rajak, *Inorg. Chem.*, **44**, 703 (2005); https://doi.org/10.1021/ic048919x
27. A.Z. El-Sonbati, A.S. Al-Shihri and A.A. El-Bindary, *J. Inorg. Organomet. Polym.*, **13**, 99 (2003); https://doi.org/10.1023/A:1024176714809
28. L. Bao, H. Liang, H. Zhang, Z. Yan, C. Sun and S. Pang, *IOP Conf. Ser. Mater. Sci. Eng.*, **772**, 012101 (2020); https://doi.org/10.1088/1757-899X/772/1/012101
29. N.H. Lam, N. Le, E.S. Kim, M.S. Tamboli, A.M. Tamboli, N.T.N. Truong and J.H. Jung, *Korean J. Chem. Eng.*, **39**, 2505 (2022); https://doi.org/10.1007/s11814-021-1024-9
30. A.K. Sutar, T. Maharana, Y. Das and P. Rath, *J. Chem. Sci.*, **126**, 1695 (2014); https://doi.org/10.1007/s12039-014-0728-3
31. M.R. Maurya, A. Chauhan, A. Verma, U. Kumar and F. Avecilla, *Catal. Today*, **388-389**, 274 (2022); https://doi.org/10.1016/j.cattod.2020.06.031
32. N. Nath, A. Routaray, Y. Das, T. Maharana and A.K. Sutar, *Kinet. Catal.*, **56**, 718 (2015); https://doi.org/10.1134/S0023158415060105
33. K.C. Gupta and A.K. Sutar, *J. Macromol. Sci. Part A Pure Appl. Chem.*, **44**, 1171 (2007); https://doi.org/10.1080/10601320701561106
34. A.K. Sutar, Y. Das, S. Pattnaik, A. Routaray, N. Nath, P. Rath and T. Maharana, *Chin. J. Catal.*, **35**, 1701 (2014); https://doi.org/10.1016/S1872-2067(14)60113-3
35. S. Kumari, P.K. Gupta, R. Karan, A. Kumar and R. Kumar, *Chem. J. Mold.*, **21**, 72 (2026); https://doi.org/10.19261/cjm.2026.1380.
36. J. He, Y. Jiang, B. Ding, Y. Wang, H. Qiu, S. Dai, X. Zhao and Z. Hou, *Appl. Catal. A Gen.*, **664**, 119351 (2023); https://doi.org/10.1016/j.apcata.2023.119351
37. T.A. Alsalim, J.S. Hadi, E.A. Al-Nasir, H.S. Abbo and S.J.J. Titinchi, *Catal. Lett.*, **136**, 228 (2010); https://doi.org/10.1007/s10562-010-0326-z